J Nanostruct 16(4): 5247-5263, Autumn 2026

RESEARCH PAPER

Study of the Gamma-Ray Attenuation Properties of Polymer Nanocomposites Reinforced with Different Materials

Athraa Mohan *, Hadi Dawyich

Department of Physics, College of Science, University of Wasit, Wasit, Iraq

ARTICLE INFO

Article History:
Received 05 May 2026
Accepted 05 July 2026
Published 01 October 2026

Keywords:
Effective atomic number
Linear attenuation coefficient
Gamma-ray shielding
PMMA
Polymer composite

ABSTRACT

In this work, the gamma-ray shielding properties of poly(methyl methacrylate) (PMMA, Perspex) composites with three different types of particulate fillers having different effective atomic number were investigated. Three types of composite material were prepared, namely containing a dispersion of zirconium borohydride, $Zr(BH_4)_4$ (A1), cadmium tungstate, $CdWO_4$ (A2) and the brass-type intermetallic compound Cu_3Zn_2 (A3) in the PMMA matrix, at loadings of 0, 5, 15, 25, 35 and 50 wt %. Bulk specimens 3 cm in diameter were prepared using dry blending, MMA-assisted consolidation and uniaxial pressing with 2-3 tons. Using the rule of mixtures, the mass attenuation coefficients were calculated using the XCOM database (version 3.1); the total linear attenuation coefficients were obtained and evaluated at the seven photon energies 0.0595, 0.093, 0.3645, 0.662, 1.173, 1.2745 and 1.332 MeV; the corresponding atomic and electronic cross sections were used to obtain the effective atomic number Z_{eff}. The results indicate that the value of μ is monotonously increasing with the content of the filler and decreasing with the photon energy. At 0.0595 MeV, μ rises from 0.2297 cm^{-1} for unfilled PMMA to 1.5369, 4.2092 and 1.9744 cm^{-1} at 50 wt % loading for A1, A2 and A3, corresponding to enhancement factors of 6.7, 18.3 and 8.6, respectively. The superior attenuator is the $CdWO_4$ system (A2) with Z_{eff} = 33.62 at 0.093 MeV, and μ = 0.1159 cm^{-1} at 1.332 MeV, while the low-Z $Zr(BH_4)_4$ system (A1) exhibits an anomalous and marginal drop in μ above 0.3645 MeV due to reduced composite electron density. The energy independent Z_{eff} is least in the Cu_3Zn_2 system (A3) with a range of 0.0595 to 1.332 MeV at 50 wt %. The trends are explained using the transition from the "low energy" photoelectric absorption ($\propto Z^{4-5}$) into "intermediate energy" Compton scattering ($\propto Z$), and PMMA–$CdWO_4$ is recognized as the most attractive lightweight, moldable alternative to lead-based shields for diagnostic and low-energy gamma applications.

How to cite this article
Mohan A, Dawyich H. Study of the Gamma-Ray Attenuation Properties of Polymer Nanocomposites Reinforced with Different Materials. J Nanostruct, 2026; 16(4):5247-5263. DOI: 10.22052/JNS.2026.04.062

INTRODUCTION

Ionizing radiation is an intrinsic hazard of nuclear power generation, diagnostic and therapeutic medicine, high-energy physics research, agriculture and a broad range of industrial processes [1-6]. Because gamma rays and X-rays are uncharged and highly penetrating, they deposit energy stochastically along their path and induce direct and indirect damage to biological tissue; limiting the delivered dose is

* *Corresponding Author Email: dhramwhan07@gmail.com*

therefore a prerequisite for the safe exploitation of nuclear technology [7,8]. Dose reduction is achieved by controlling exposure time, increasing the source-to-observer distance and interposing a shield, the last of which is the only measure that can be engineered arbitrarily to a prescribed attenuation level [8,9].

The performance of a shield is governed by the probability of photon interaction per unit path length in the absorbing medium, which in turn depends on the incident photon energy, the atomic number of the constituent elements and the bulk density of the material [9-13]. Conventional shields based on lead and lead-loaded concrete provide high attenuation per unit thickness, but their weight, brittleness, toxicity and poor formability restrict their use in wearable, portable and medical geometries. Consequently, considerable effort has been directed toward polymer matrices loaded with high-atomic-number particulate fillers, which combine low density and ease of moulding with an electron density that can be tuned through the filler fraction [14,15].

A composite is a material formed by combining two or more constituents that differ in composition or form at the macroscopic scale in order to obtain a property set unattainable from either phase alone, and consists of a continuous matrix and a dispersed reinforcement [16,17]. Poly(methyl methacrylate) (PMMA, Perspex) is an attractive matrix for shielding applications because it is optically transparent, chemically stable, inexpensive, readily cold-pressed and hydrogen-rich, the last property being advantageous where mixed neutron–gamma fields are encountered [18-22]. Its intrinsic gamma-ray attenuation, however, is low, so its shielding capability must be raised by reinforcement.

In the present work three particulate fillers spanning a wide range of atomic number were selected in order to separate the roles of electron density and atomic number in the attenuation process: the low-Z hydrogen-rich hydride $Zr(BH_4)_4$, the high-Z scintillator compound $CdWO_4$ (Z_W = 74, Z_{Cd} = 48) and the intermediate-Z intermetallic Cu_3Zn_2 (Z_Cu = 29, Z_Zn = 30). Each filler was

Fig. 1. Agate/ceramic mortar and pestle used for the dry homogenization of the filler powders prior to polymer incorporation.

Table 1. Composition of the prepared composite samples.

Sample ID	Description
A1	Perspex ($C_5H_8O_2$+ $Zr(BH_4)_4$
A2	Perspex ($C_5H_8O_2$+ $CdWO_4$
A3	Perspex + Cu_3Zn_2

incorporated into PMMA at 0, 5, 15, 25, 35 and 50 wt %, giving eighteen distinct formulations. The total linear attenuation coefficient and the effective atomic number were determined from the XCOM/WinXCOM photon cross-section database [23] between 1 keV and 100 GeV, with particular attention to the seven energies emitted by the reference sources ^{241}Am, ^{137}Cs and ^{60}Co, and the resulting trends are interpreted in terms of the dominant photon interaction mechanism in each energy regime.

MATERIALS AND METHODS

Materials

PMMA powder (Perspex) as the polymer matrix, Zr (BH4)4 powder, Perspex powder, $CdWO_4$ powder, Cu_3Zn_2 powder, PMMA liquid monomer (Methyl Methacrylate, MMA) as the curing agent (hardener), Ethanol (analytical grade) for wet mixing, Steel mold (3 cm diameter), Hydraulic press.

Experimental Procedure

The following steps were applied for the preparation of all samples:

1. Weighing: Each component was weighed accurately according to the compositions listed in Table 1. The total mass of every sample was fixed at 12 g, consisting of PMMA as the matrix and the corresponding filler system.

2. Dry Mixing: The filler components were mixed in a ceramic mortar for 10–15 minutes to ensure uniform distribution.

3. Polymer Incorporation: PMMA powder was added to the filler mixture and blended thoroughly for an additional 10 minutes. A few drops of PMMA liquid monomer (Methyl Methacrylate, MMA), which acts as the hardener, were added gradually to obtain a homogeneous paste. Typically, 2–4 drops of MMA were used per gram of PMMA, depending on viscosity.

4. Molding: The paste was transferred into a stainless-steel mold of 3 cm diameter. The mold was lightly coated with a release agent to prevent sticking. Gentle tapping was applied to remove entrapped air.

5. Pressing: The samples were pressed using a hydraulic press at a load of 2–3 tons for 10–15 minutes to ensure proper compaction and adhesion within the polymer matrix.

6. Curing: The molded samples were allowed to cure at room temperature. Optional mild heating (40–60°C) was applied to accelerate polymerization of the PMMA–MMA system.

7. Demolding: After complete curing, the samples were removed carefully from the mold and stored in sealed containers to avoid moisture uptake.

Fig. 2. Stainless-steel die, 3 cm in internal diameter, used for cold compaction of the composite discs.

RESULTS AND DISCUSSION

Characterization of the Prepared Composites

Morphological Characterization by FE-SEM

The morphology and the size distribution of the dispersed phase were examined with a MIRA3 TESCAN field-emission scanning electron microscope operated in secondary-electron mode at an accelerating voltage of 15.0 kV and

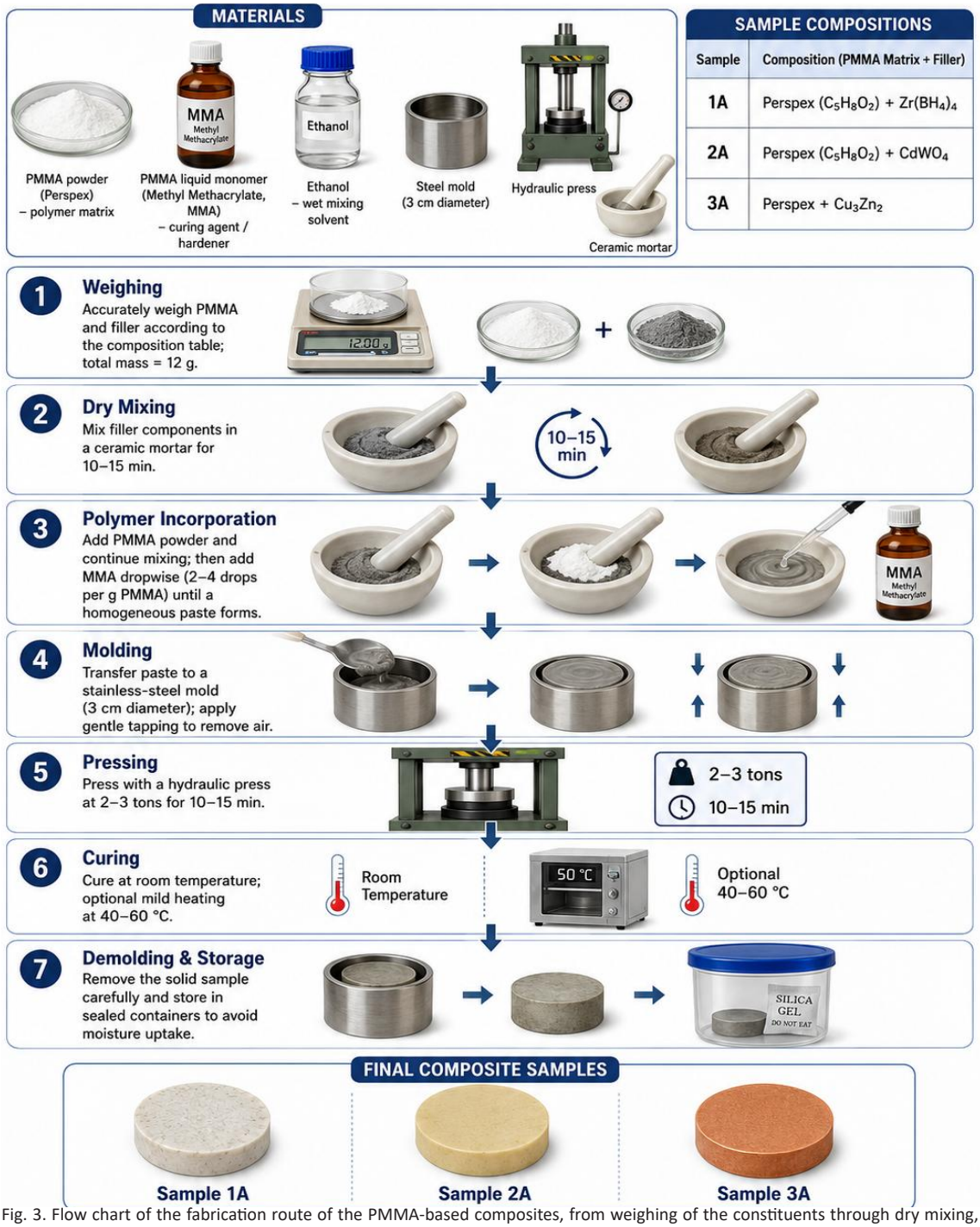

Fig. 3. Flow chart of the fabrication route of the PMMA-based composites, from weighing of the constituents through dry mixing, MMA-assisted polymer incorporation, moulding, uniaxial pressing, curing and demoulding, together with the compositions of the three sample groups.

a working distance of 5.69 mm. Fig. 4 shows the fracture surfaces of the three composites at two magnifications, 95 kx and 135 kx, the second magnification being used to verify the size statistics obtained at the lower one.

In sample A1 the $Zr(BH_4)_4$ phase appears as quasi-spherical nodules uniformly decorating the PMMA fracture surface, with measured diameters of 41–66 nm (mean 55.0 nm) at 95 kx and 42–63 nm (mean 53.4 nm) at 135 kx. Sample A2 contains well-defined faceted, cuboidal $CdWO_4$ crystallites of 52–82 nm (mean 68.2 nm) and 54–78 nm (mean 67.0 nm) at the two magnifications, the sharp crystal habit reflecting the high crystallinity

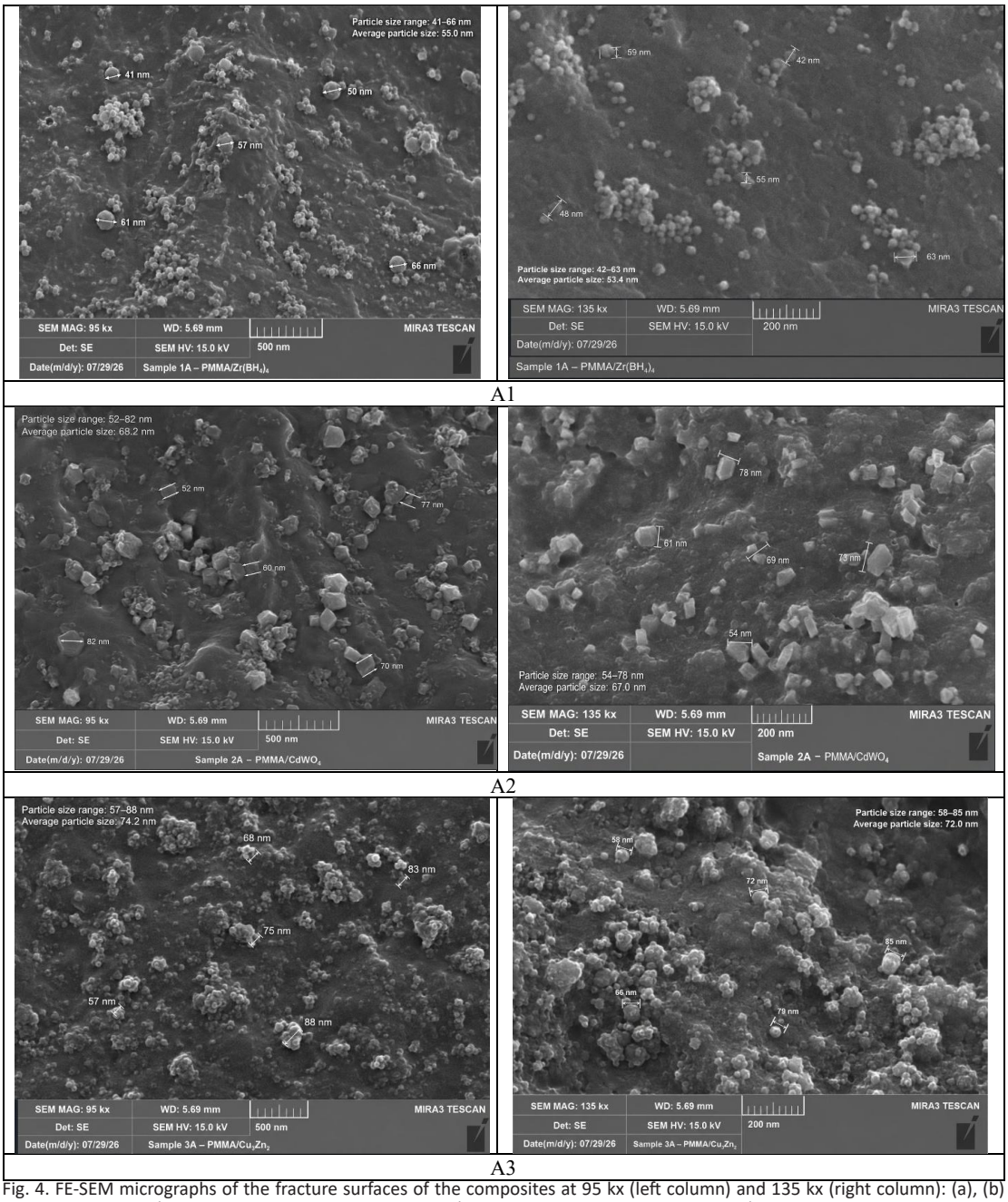

Fig. 4. FE-SEM micrographs of the fracture surfaces of the composites at 95 kx (left column) and 135 kx (right column): (a), (b) sample A1 ($PMMA/Zr(BH_4)_4$); (c), (d) sample A2 ($PMMA/CdWO_4$); (e), (f) sample A3 ($PMMA/Cu_3Zn_2$). Representative particle dimensions are indicated on each micrograph.

of the tungstate. In sample A3 the Cu_3Zn_2 filler occurs as cauliflower-like agglomerates built from spheroidal primary particles of 57–88 nm (mean 74.2 nm) and 58–85 nm (mean 72.0 nm). The agreement between the two magnifications, better than 3 % in the mean particle size for every sample, confirms that the reported statistics are representative of the bulk microstructure.

Three conclusions of direct relevance to the shielding behaviour follow from these observations. First, all three fillers lie in the nanometric range below 100 nm, so the

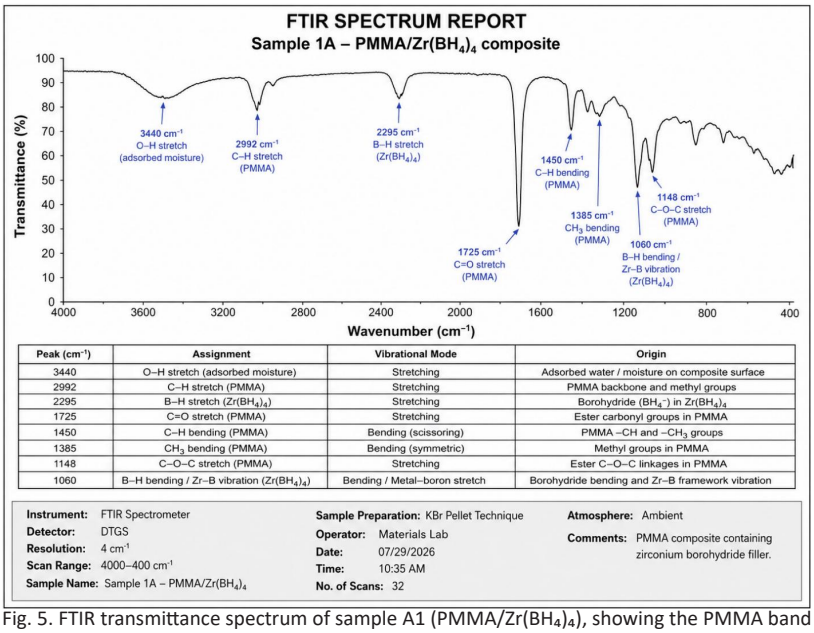

Peak (cm⁻¹)	Assignment	Vibrational Mode	Origin
3440	O–H stretch (adsorbed moisture)	Stretching	Adsorbed water / moisture on composite surface
2992	C–H stretch (PMMA)	Stretching	PMMA backbone and methyl groups
2295	B–H stretch ($Zr(BH_4)_4$)	Stretching	Borohydride (BH_4^-) in $Zr(BH_4)_4$
1725	C=O stretch (PMMA)	Stretching	Ester carbonyl groups in PMMA
1450	C–H bending (PMMA)	Bending (scissoring)	PMMA –CH and $–CH_3$ groups
1385	CH_3 bending (PMMA)	Bending (symmetric)	Methyl groups in PMMA
1148	C–O–C stretch (PMMA)	Stretching	Ester C–O–C linkages in PMMA
1060	B–H bending / Zr–B vibration ($Zr(BH_4)_4$)	Bending / Metal–boron stretch	Borohydride bending and Zr–B framework vibration

Instrument: FTIR Spectrometer
Detector: DTGS
Resolution: 4 cm^{-1}
Scan Range: 4000–400 cm^{-1}
Sample Name: Sample 1A – PMMA/$Zr(BH_4)_4$
Sample Preparation: KBr Pellet Technique
Operator: Materials Lab
Date: 07/29/2026
Time: 10:35 AM
No. of Scans: 32
Atmosphere: Ambient
Comments: PMMA composite containing zirconium borohydride filler.

Fig. 5. FTIR transmittance spectrum of sample A1 (PMMA/$Zr(BH_4)_4$), showing the PMMA band set together with the B–H stretching and Zr–B vibrations of the borohydride filler.

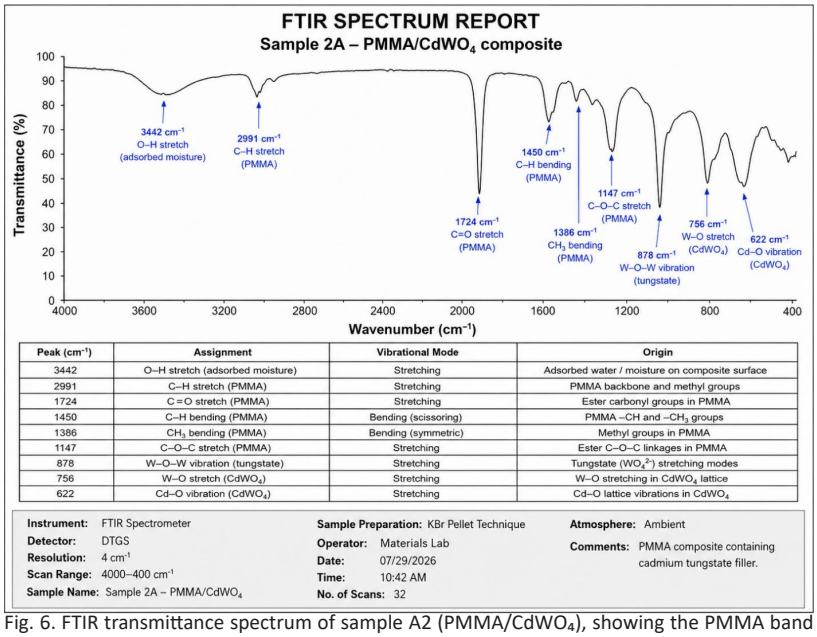

Peak (cm⁻¹)	Assignment	Vibrational Mode	Origin
3442	O–H stretch (adsorbed moisture)	Stretching	Adsorbed water / moisture on composite surface
2991	C–H stretch (PMMA)	Stretching	PMMA backbone and methyl groups
1724	C=O stretch (PMMA)	Stretching	Ester carbonyl groups in PMMA
1450	C–H bending (PMMA)	Bending (scissoring)	PMMA –CH and $–CH_3$ groups
1386	CH_3 bending (PMMA)	Bending (symmetric)	Methyl groups in PMMA
1147	C–O–C stretch (PMMA)	Stretching	Ester C–O–C linkages in PMMA
878	W–O–W vibration (tungstate)	Stretching	Tungstate (WO_4^{2-}) stretching modes
756	W–O stretch ($CdWO_4$)	Stretching	W–O stretching in $CdWO_4$ lattice
622	Cd–O vibration ($CdWO_4$)	Stretching	Cd–O lattice vibrations in $CdWO_4$

Instrument: FTIR Spectrometer
Detector: DTGS
Resolution: 4 cm^{-1}
Scan Range: 4000–400 cm^{-1}
Sample Name: Sample 2A – PMMA/$CdWO_4$
Sample Preparation: KBr Pellet Technique
Operator: Materials Lab
Date: 07/29/2026
Time: 10:42 AM
No. of Scans: 32
Atmosphere: Ambient
Comments: PMMA composite containing cadmium tungstate filler.

Fig. 6. FTIR transmittance spectrum of sample A2 (PMMA/$CdWO_4$), showing the PMMA band set together with the W–O–W, W–O and Cd–O vibrations of the tungstate filler.

materials are properly described as polymer nanocomposites; the associated high specific surface area and small interparticle spacing produce a dense, spatially uniform population of attenuating centres and suppress the filler-free channels through which photons could otherwise stream with reduced probability of interaction. Second, the mean particle size increases in the sequence A1 < A2 < A3, which follows the increasing density and the stronger magnetostatic and van der Waals agglomeration tendency of the metallic filler, and which explains the slightly coarser dispersion observed in A3. Third, the micrographs reveal neither macroscopic voids nor extensive particle pull-out at the fracture surface, indicating adequate wetting of the particles by the PMMA–MMA system and hence a compact body whose measured bulk density is consistent with the rule-of-mixtures density used in the attenuation calculations. Since the particle dimensions are smaller than the photon mean free path in the composite by four to five orders of magnitude, the specimens act as an effectively homogeneous medium for the incident gamma photons, which is precisely the assumption underlying the mixture rule and therefore validates the XCOM-based evaluation presented in the following sections.

Functional-Group Analysis by FTIR Spectroscopy

The chemical integrity of the matrix and of the dispersed fillers was examined by Fourier-transform infrared spectroscopy in transmittance mode (KBr-pellet technique, DTGS detector, spectral resolution 4 cm^{-1}, 32 accumulated scans, scan range 4000–400 cm^{-1}, ambient atmosphere). The spectra of samples A1, A2 and A3 are presented in Figs. 5–7, respectively, each accompanied by the assignment of its principal absorption bands.

The three spectra are dominated by the characteristic absorption bands of the PMMA matrix: a broad O–H stretching envelope at 3438–3442 cm^{-1} arising from moisture adsorbed on the specimen surface, C–H stretching of the backbone and methyl groups at 2991–2992 cm^{-1}, the intense ester carbonyl (C=O) stretch at 1724–1725 cm^{-1}, C–H scissoring at 1450–1451 cm^{-1}, symmetric CH_3 bending at 1384–1386 cm^{-1} and the ester C–O–C stretch at 1147–1148 cm^{-1}. The persistence of this

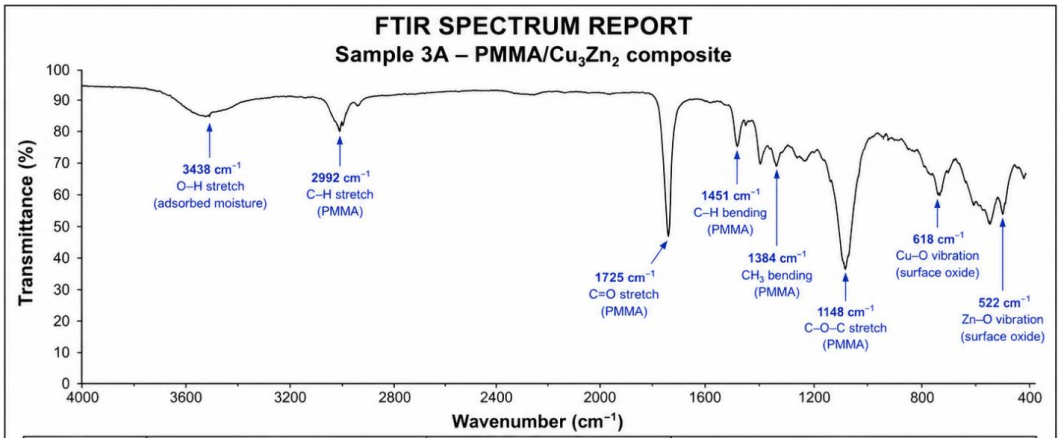

Peak (cm^{-1})	Assignment	Vibrational Mode	Origin
3438	O–H stretch (adsorbed moisture)	Stretching	Adsorbed water / moisture on composite surface
2992	C–H stretch (PMMA)	Stretching	PMMA backbone and methyl groups
1725	C=O stretch (PMMA)	Stretching	Ester carbonyl groups in PMMA
1451	C–H bending (PMMA)	Bending (scissoring)	PMMA –CH and –CH_3 groups
1384	CH_3 bending (PMMA)	Bending (symmetric)	Methyl groups in PMMA
1148	C–O–C stretch (PMMA)	Stretching	Ester C–O–C linkages in PMMA
752	Metal–O vibration (Cu_3Zn_2 surface)	Bending / Lattice vibration	Metal–oxygen vibration of Cu_3Zn_2 surface oxides
618	Cu–O vibration (surface oxide)	Stretching / Bending	Copper-oxygen vibration from surface oxide
522	Zn–O vibration (surface oxide)	Stretching / Bending	Zinc–oxygen vibration from surface oxide

Instrument: FTIR Spectrometer
Detector: DTGS
Resolution: 4 cm^{-1}
Scan Range: 4000–400 cm^{-1}
Sample Name: Sample 3A – PMMA/Cu_3Zn_2
Sample Preparation: KBr Pellet Technique
Operator: Materials Lab
Date: 07/29/2026
Time: 10:48 AM
No. of Scans: 32
Atmosphere: Ambient
Comments: PMMA composite containing Cu_3Zn_2 metallic filler with weak surface oxide vibrations.

Fig. 7. FTIR transmittance spectrum of sample A3 (PMMA/Cu_3Zn_2) recorded from 4000 to 400 cm^{-1}, with the identified matrix bands and the weak Cu–O and Zn–O surface-oxide vibrations.

band set at essentially unshifted wavenumbers in all three composites demonstrates that the polymer backbone is chemically intact after mixing, pressing and curing, and that filler incorporation proceeds by physical dispersion rather than by chemical attack on the matrix. The absence of a strong vinylic C=C absorption near 1640 cm^{-1} further indicates that the MMA hardener has been essentially completely polymerized, so that no residual monomer remains to plasticize the composite or to alter its density.

Superimposed on the matrix signature, each spectrum exhibits the vibrational fingerprint of its own filler. In sample A1 the band at 2295 cm^{-1} is assigned to the B–H stretching mode of the borohydride anion, and the feature at 1060 cm^{-1} to B–H bending coupled with Zr–B framework vibration; their appearance confirms that the moisture-sensitive $Zr(BH_4)_4$ phase survived processing without hydrolysis, which is significant because loss of the BH_4^- groups would reduce both the hydrogen content and the density on which the calculated attenuation coefficients depend. In sample A2 the bands at 878, 756 and 622 cm^{-1} correspond to W–O–W bridging vibrations, W–O stretching and Cd–O lattice vibrations, verifying that the tungstate (WO_4^{2-}) group and hence the stoichiometry of $CdWO_4$ are preserved. In sample A3 only weak absorptions at 752, 618 and 522 cm^{-1}, attributable to metal–oxygen, Cu–O and Zn–O vibrations of thin surface oxide layers, are detected, which is consistent with a predominantly metallic Cu_3Zn_2 filler carrying no more than a native passivating oxide film.

The small displacements (1–2 cm^{-1}) and the slight broadening of the carbonyl band relative to unfilled PMMA are indicative of weak dipolar and hydrogen-bonding interactions between the polar ester groups of the matrix and the filler surfaces, that is, of physical rather than covalent interfacial coupling. Such interaction is sufficient to immobilize the nanoparticles and to inhibit their sedimentation during curing, while leaving the processability of PMMA unaffected. From the standpoint of the shielding calculation, the FTIR results are essential validation evidence: because the XCOM computation is performed on the nominal elemental weight fractions of each formulation, the conclusion that both matrix and fillers retain their stoichiometry after fabrication justifies the application of the mixture rule to the real specimens.

Theoretical Basis

Total Linear Attenuation Coefficient

In shielding design materials, the linear attenuation coefficient (μ) that can be defined as the likelihood of radiation to interact with a substance per unit path length is, a significant quantity and its values depend on the energy of the incident photon and, the atomic number of the material, and the density (ρ) of the shielding medium [19]. In addition to that, the mass attenuation coefficient (μ/rho) ($cm^2.g^{-1}$) is a direct measure of the effectiveness of a shielding material, relative to unit mass of material. In general, the mass attenuation coefficient computation in or around high energies is generally highly required and utilized as a radiation shielding design database of radiation sources, reactors and particle accelerators [20]. The nature of the interaction of photons with matter is different when compared to other forms of radiation, such as charged particles. When photons pass through a material, some are absorbed, while others pass through without any interaction. The remaining photons scatter in different directions after losing some of their intensity [18]. If we consider a beam of photons of known intensity (I_0) passing through a shield of thickness (x), multiple interactions will occur between the photons and the atoms of the shielding material. These interactions result in a change in the beam intensity due to absorption and attenuation. The thicker the shielding material, the greater the attenuation and absorption the beam experiences. Therefore, there is an inverse relationship between the thickness of the material and the intensity of the radiation. Mathematically, the change in radiation intensity can be expressed by dI, and the thickness of the shielding material is denoted by dx (Eq. 1) [14].

$$-\frac{dI}{I} = (\mu)dx \tag{1}$$

Where μ is the linear attenuation coefficient.

By integrating this equation as follows (Eqs. 2 and 3) [15]:

$$\int_{I_0}^{I} \frac{dI}{I} = \int_{0}^{x} -(\mu)dx \tag{2}$$

$$\text{Ln } I(x)-\text{Ln } I0=-(\mu)\, x \quad (3)$$

From the exponential equation, the attenuation coefficient was calculated over an unlimited range of energies (Eq. 4).

$$I_x= I_0\, e^{-\mu x} \quad (4)$$

The linear attenuation coefficient is an important parameter in the calculations of shielding used in radiation protection, especially when expressing the power of a photon as it moves through and passes through the absorbing medium. Another parameter is the mass attenuation coefficient (μm) in units of (cm^2/g) and its relationship to the linear attenuation coefficient μ(cm^{-1}) (Eq. 5)[16]:

$$\mu(cm^{-1}) =\mu_m(cm^2/g) * \rho(g/cm^3) \quad (5)$$

ρ: Density of the intercepting medium in units (cm^3/g)

The total photon mass attenuation coefficient $(\mu/\rho)_{comp}$ has been estimated by the following 'mixture rule' with WinXCOM program for a chemical compound or mixture (Eq. 6):

$$(\mu/\rho)_{compound}=\sum_i (\mu/\rho)_i\, W_i \quad (6)$$

where ωi is the weight fraction of the ith constituent element present in the given compound and i (μ / ρ) is the photon mass attenuation. For a material composed of multi elements the fraction by weight is given by Eq. 7:

$$W_i=n_iA_i/\sum_i n_i\, A \quad (7)$$

ni: the number of atoms of each element in the compound.

Ai: the mass number of each element in the compound.

The mass attenuation coefficient depends on the photon energy and the atomic number of the intercepting medium (Z)[17].

The total linear attenuation coefficients (μ) were obtained as the results obtained during calculations of XCOM by using density (ρ) of the shield materials. The rule of mixtures formula was used to compute the density of composite materials using the Eq. 8 [21]:

$$\rho_c = V_f\, \rho_f +(1 -V_f)\, \rho_m \quad (8)$$

Where: ρ_c, ρ_f, ρ_m Density of composite body, reinforcement and the matrix materials respectively. : Vf Fractional volume for reinforcement material [22].

Effective Atomic Number (Z_{eff})

Is also important for selecting a substitute material in radiation shielding. It is defined as an atomic number corresponding to a mixture or compound which interacts with photons in a way that is equivalent to a single elemental substance with this atomic number interacting with photons It is a particularly important parameter in the fields of radiation shielding design and absorbed dose calculations in radiotherapy [15]. The effective atomic number is not a constant for a given material, but rather a variable that changes with photon energy and depends on the reaction processes taking place and the proportion of each element within the composite material. Zeff is calculated by Eqs. 9-13:

$$\sigma_m = (\mu_m)_{comP} \frac{\sum_i n_i A_i}{N_A} \quad (9)$$

$$\sigma_a = \frac{\sigma_m}{\sum_i n_i} \quad (10)$$

$$\sigma_{el} = \frac{1}{N_A} \sum \frac{f_i A_i}{Z_i} (\mu_m)_i \quad (11)$$

$$Z_{componut} = \frac{\sigma_a}{\sigma_{el}} \quad (12)$$

$$Z_{eff} = \sum_{i=1}^{2} W_i Z_i \quad (13)$$

σ_a: atomic cross section, σm: mass cross section, σ_{el}:Electron cross section, N_A: Avogadro's number, Zi: Atomic number of each element in the compound (for all base elements), Zcomp: Atomic number of the compound, Wi: Weight fraction of each element (the weight ratio of each element in the compound), if: Number of atoms of element (i) to the total number of atoms of the elements

present in the compound, Ai: Atomic weight (mass number) of each element in the compound, (μm): Raw materials for compounds, (μm)i: Conventional mass attenuation of each element in the compound.

Gamma-Ray Shielding Results and Discussion

Total Linear Attenuation Coefficient

The total linear attenuation coefficients of the eighteen formulations, obtained from the XCOM mass attenuation coefficients and the rule-of-mixtures densities, are listed in Table 2 and displayed in Figs. 8 and 9. Two general trends are common to the three groups: μ increases with the filler content at low photon energy, and μ decreases monotonically with increasing photon energy at every concentration. The values recorded at 0.0595 and 0.093 MeV are up to one

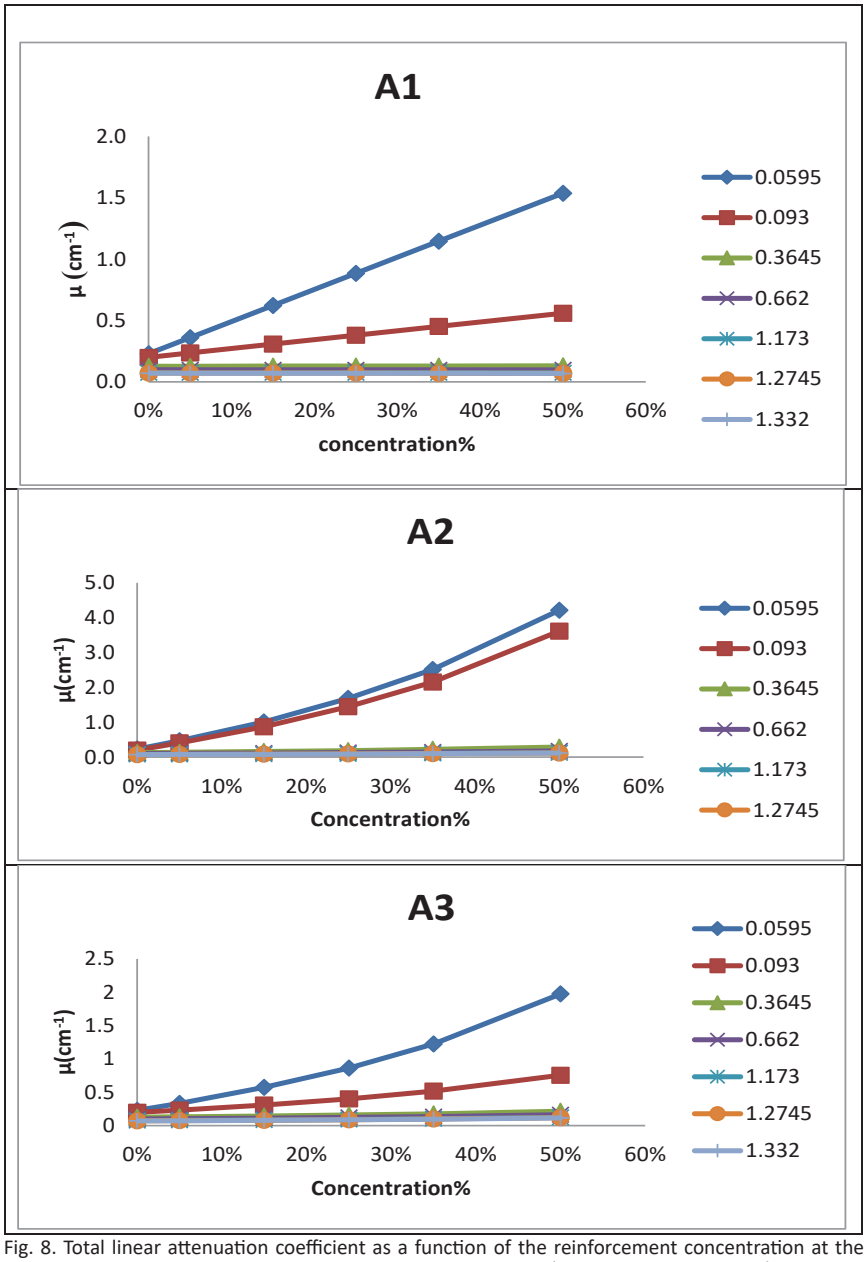

Fig. 8. Total linear attenuation coefficient as a function of the reinforcement concentration at the seven investigated photon energies for group A: (a) A1, PMMA/$Zr(BH_4)_4$; (b) A2, PMMA/$CdWO_4$; (c) A3, PMMA/Cu_3Zn_2.

order of magnitude larger than those obtained above 0.3645 MeV, which reflects the change of the dominant photon interaction mechanism across the energy range examined.

Sample A2 (PMMA/$CdWO_4$) is the most efficient attenuator at every energy and at every loading. Its coefficient at 0.0595 MeV rises from 0.2297 cm^{-1} for the unfilled matrix to 0.4688, 1.0086, 1.6830, 2.5113 and 4.2092 cm^{-1} at 5, 15, 25, 35 and 50 wt %, an eighteen-fold enhancement, and it remains superior at 1.332 MeV (0.1159 cm^{-1} against 0.0708 cm^{-1} for pure PMMA). This behaviour is a direct consequence of the high atomic numbers of tungsten (Z = 74) and cadmium (Z = 48) and of the high crystallographic density of $CdWO_4$, both of which raise the electron density of the composite

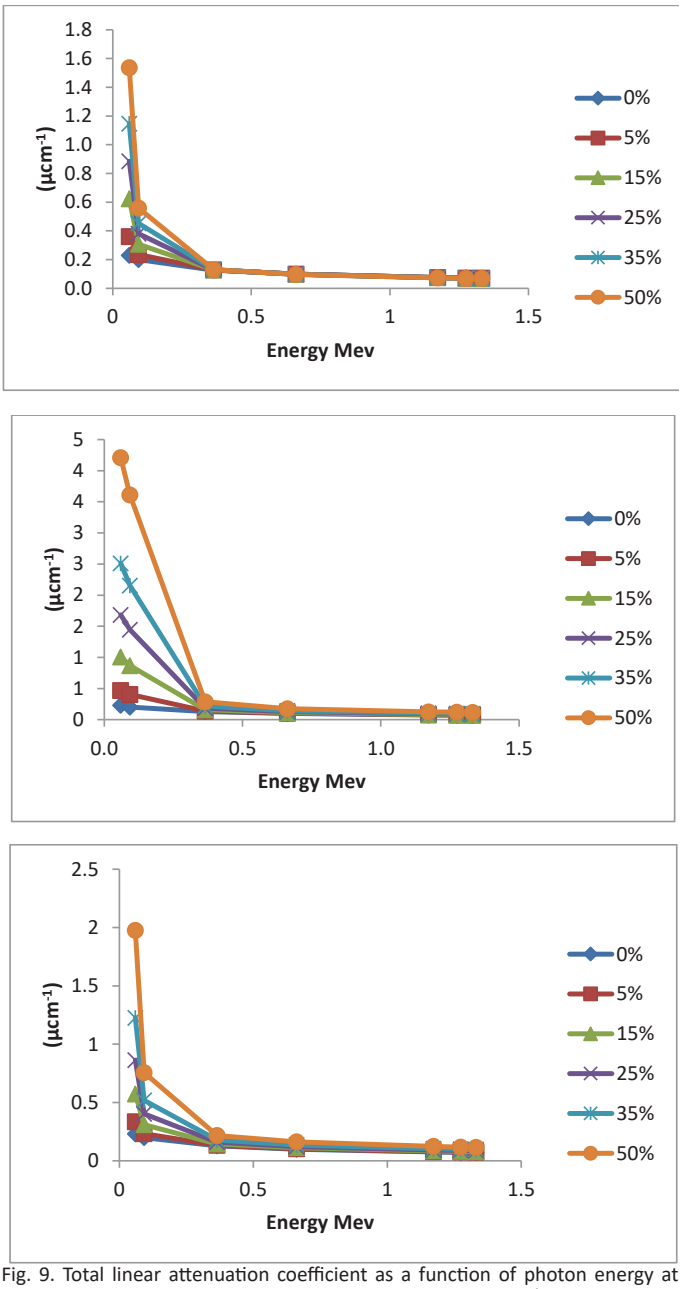

Fig. 9. Total linear attenuation coefficient as a function of photon energy at the different filler concentrations for group A: (a) A1, PMMA/$Zr(BH_4)_4$; (b) A2, PMMA/$CdWO_4$; (c) A3, PMMA/Cu_3Zn_2.

and hence the photoelectric cross section, which scales approximately as Z^{4-5}/E^3.

Sample A3 (PMMA/Cu_3Zn_2) occupies an intermediate position, its coefficient at 0.0595 MeV increasing from 0.2297 to 1.9744 cm^{-1} at 50 wt %, and, in contrast to A1, it continues to improve over the whole energy range (0.0708 → 0.1154 cm^{-1} at 1.332 MeV) because the intermediate atomic numbers of copper (Z = 29) and zinc (Z = 30) combine with a density high enough to increase the Compton electron density of the matrix.

Sample A1 (PMMA/$Zr(BH_4)_4$) shows a distinctive dual behaviour that deserves particular attention. Below 0.1 MeV the addition of the filler is strongly beneficial, μ reaching 1.5369 cm^{-1} at 0.0595 MeV and 50 wt % against 0.2297 cm^{-1} for the unfilled matrix, owing to the photoelectric contribution of zirconium (Z = 40). Above 0.3645 MeV, however, the trend reverses and μ decreases slightly with increasing filler content (0.0991 → 0.0975 cm^{-1} at 0.662 MeV and 0.0708 → 0.0687 cm^{-1} at 1.332 MeV for 0 → 50 wt %). In this energy region Compton scattering dominates and the attenuation per unit length is governed by the electron density rather than by Z; because each $Zr(BH_4)_4$ formula unit carries sixteen hydrogen and four boron atoms,

Table 2. Total linear attenuation coefficient μ (cm^{-1}) of the group-A composites at the investigated filler concentrations and photon energies.

Group	Energy (MeV)	μ (cm^{-1})					
		0%	5%	15%	25%	35%	50%
A1	0.0595	0.2297	0.3609	0.6229	0.8846	1.1458	1.5369
	0.093	0.1994	0.2355	0.3077	0.3796	0.4516	0.5592
	0.3645	0.1272	0.1276	0.1284	0.1291	0.1298	0.1308
	0.662	0.0991	0.0990	0.0986	0.0983	0.0980	0.0975
	1.173	0.0755	0.0753	0.0749	0.0745	0.0740	0.0734
	1.2745	0.0724	0.0722	0.0718	0.0713	0.0709	0.0703
	1.332	0.0708	0.0705	0.0701	0.0697	0.0693	0.0687

Group	Energy (MeV)	μ (cm^{-1})					
		0%	5%	15%	25%	35%	50%
A2	0.0595	0.2297	0.4688	1.0086	1.6830	2.5113	4.2092
	0.093	0.1994	0.4043	0.8669	1.4451	2.1540	3.6115
	0.3645	0.1272	0.1370	0.1577	0.1858	0.2193	0.2877
	0.662	0.0991	0.1038	0.1135	0.1273	0.1433	0.1763
	1.173	0.0755	0.0785	0.0845	0.0934	0.1035	0.1244
	1.2745	0.0724	0.0752	0.0809	0.0893	0.0989	0.1187
	1.332	0.0708	0.0735	0.0790	0.0872	0.0966	0.1159

Group	Energy (MeV)	μ (cm^{-1})					
		0%	5%	15%	25%	35%	50%
A3	0.0595	0.2297	0.3336	0.5721	0.8632	1.2256	1.9744
	0.093	0.1994	0.2325	0.3086	0.4014	0.5170	0.7560
	0.3645	0.1272	0.1325	0.1446	0.1595	0.1777	0.2159
	0.662	0.0991	0.1029	0.1116	0.1223	0.1356	0.1630
	1.173	0.0755	0.0783	0.0848	0.0928	0.1027	0.1231
	1.2745	0.0723	0.0751	0.0813	0.0890	0.0984	0.1180
	1.332	0.0708	0.0734	0.0795	0.0870	0.0962	0.1154

the electron-to-mass ratio of the composite falls when the borohydride replaces the hydrogen-rich but oxygen-bearing PMMA, and the small loss of Compton scattering centres outweighs the modest photoelectric gain contributed by zirconium. The $Zr(BH_4)_4$ system is therefore recommended only for low-energy photon fields, or for mixed neutron–gamma fields where its high hydrogen and boron content provides simultaneous neutron moderation and capture.

Fig. 9 shows the corresponding energy dependence. The steep fall of μ between 0.0595 and 0.3645 MeV, followed by a slow, almost linear decay up to 1.332 MeV, marks the hand-over from photoelectric absorption to Compton scattering; none of the formulations reaches the pair-production threshold (1.022 MeV) with sufficient margin for that process to contribute appreciably at the energies studied. The curves also converge at high energy, confirming that the benefit obtained by loading a polymer with a high-Z filler is large at diagnostic energies and progressively smaller as the photon energy increases.

Taken together, the attenuation data rank the three systems as A2 > A3 > A1 at all energies above 0.1 MeV, and A2 > A3 > A1 also in the low-

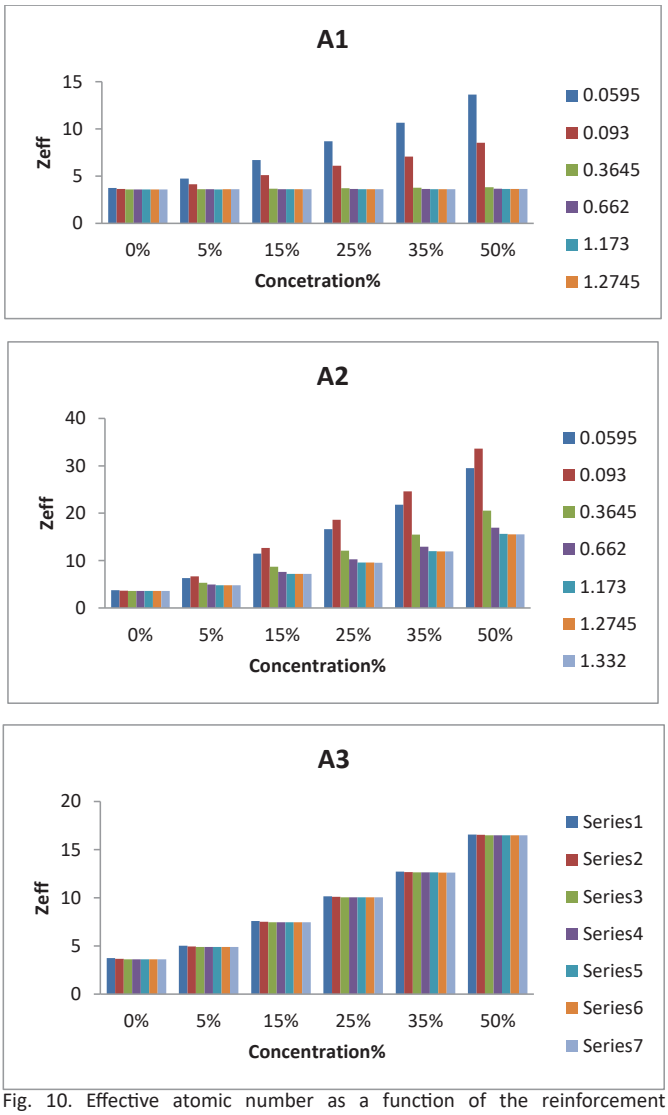

Fig. 10. Effective atomic number as a function of the reinforcement concentration at the seven investigated photon energies for group A: (a) $PMMA/Zr(BH_4)_4$; (b) $PMMA/CdWO_4$; (c) $PMMA/Cu_3Zn_2$.

energy region, the ranking being governed by the product of the filler atomic number and its volumetric loading. The enhancement of μ with concentration is superlinear for A2, reflecting the simultaneous increase of both the density and the effective atomic number of that composite.

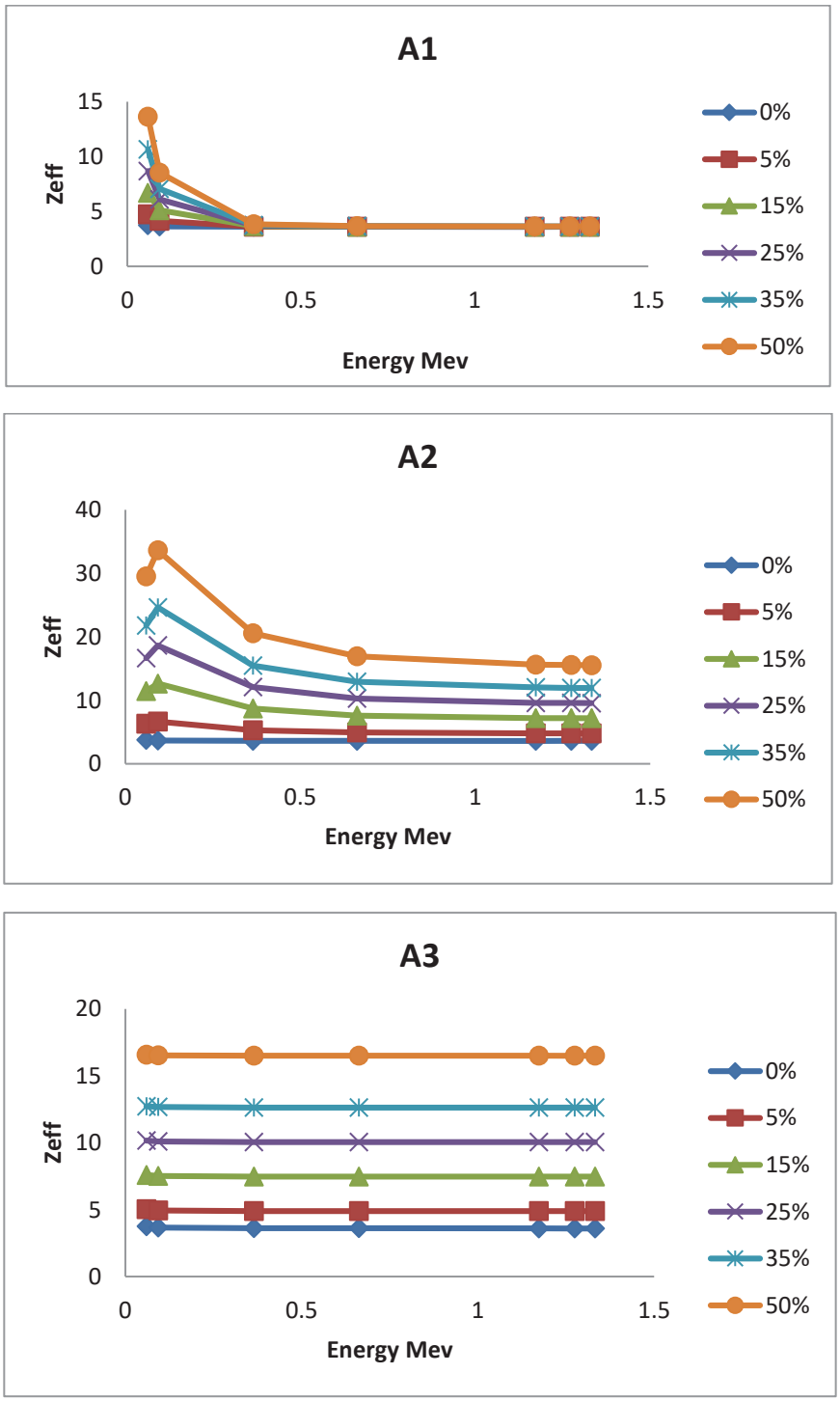

Fig. 11. Effective atomic number as a function of photon energy at the different filler concentrations for group A: (a) PMMA/$Zr(BH_4)_4$; (b) PMMA/$CdWO_4$; (c) PMMA/Cu_3Zn_2.

Effective Atomic Number

Fig. 10 shows that Z_eff increases monotonically with the reinforcement concentration in all three systems, since the addition of elements whose atomic number exceeds that of the light constituents of PMMA (H, C, O) raises the weighted electronic cross section of the mixture. At 0.093 MeV and 50 wt % loading, Z_eff attains 8.54 for A1, 33.62 for A2 and 16.54 for A3, compared with 3.65 for the unfilled matrix. Because both the photoelectric cross section and, at higher energies, the number of scattering electrons per unit volume grow with Z_eff, the increase of the effective atomic number is the physical origin of the increase in the linear attenuation coefficient reported in Table 2.

The magnitude of the increase, however, is strongly filler-dependent. The gain is largest for the $CdWO_4$ system, in which the heavy tungsten and cadmium atoms carry a large weight fraction, moderate for the Cu_3Zn_2 system, and smallest for $Zr(BH_4)_4$, in which each zirconium atom is accompanied by twenty light boron and hydrogen atoms. In the latter case the heavy-atom contribution is diluted by the light constituents of the borohydride, so that the composite gains comparatively little in effective atomic number and, above 0.3645 MeV, loses electron density; this explains quantitatively the anomalous decrease of μ with concentration observed for A1 in that energy range.

The energy dependence of Z_eff is presented in Fig. 11 and reveals three distinct patterns. For A1, Z_eff is high at 0.0595–0.093 MeV, particularly at 50 wt % (13.63 and 8.54), and then falls sharply to an essentially constant value of about 3.64 above 0.3645 MeV; the photoelectric effect, whose cross section varies as Z^{4-5}, strongly weights the zirconium contribution at low energy, whereas the Compton cross section varies only linearly

Table 3. Effective atomic number Z_{eff} of the group-A composites at the investigated filler concentrations and photon energies.

Croup Name	Energy (MeV)	Zeff					
		0%	5%	15%	25%	35%	50%
$C_5H_8O_2$+$Zr(BH_4)_4$	0.0595	3.745602	4.73436	6.711877	8.689393	10.66691	13.63319
	0.093	3.651855	4.141044	5.119422	6.097801	7.076179	8.543747
	0.3645	3.602237	3.625727	3.672707	3.719687	3.766666	3.837136
	0.662	3.601563	3.609468	3.625278	3.641088	3.656898	3.680613
	1.173	3.600631	3.604359	3.611816	3.619272	3.626728	3.637913
	1.2745	3.600992	3.604658	3.61199	3.619321	3.626653	3.637651
	1.332	3.601076	3.604718	3.612003	3.619287	3.626572	3.637499
$C_5H_8O_2$+$CdWO_4$	0.0595	3.745602	6.322104	11.47511	16.62811	21.78112	29.51062
	0.093	3.651855	6.649021	12.64335	18.63769	24.63202	33.62352
	0.3645	3.602237	5.298355	8.690589	12.08282	15.47506	20.56341
	0.662	3.601563	4.934314	7.599815	10.26532	12.93082	16.92907
	1.173	3.600631	4.802844	7.207271	9.611697	12.01612	15.62276
	1.2745	3.600992	4.795681	7.18506	9.57444	11.96382	15.54789
	1.332	3.601076	4.793272	7.177665	9.562057	11.94645	15.52304
$C_5H_8O_2$+Cu_3Zn_2	0.0595	3.745602	5.028969	7.595705	10.16244	12.72918	16.57928
	0.093	3.651855	4.940366	7.517389	10.09441	12.67143	16.53697
	0.3645	3.602237	4.892354	7.472587	10.05282	12.63305	16.5034
	0.662	3.601563	4.891598	7.471667	10.05174	12.63181	16.50191
	1.173	3.600631	4.890709	7.470864	10.05102	12.63117	16.50141
	1.2745	3.600992	4.890833	7.470514	10.0502	12.62988	16.4994
	1.332	3.601076	4.890912	7.470583	10.05025	12.62993	16.49943

with Z, so the composite reverts to a behaviour dominated by its light matrix. For A2, Z_eff remains high over the entire range, decreasing from 29.51 at 0.0595 MeV to 15.52 at 1.332 MeV at 50 wt % while passing through a maximum of 33.62 at 0.093 MeV; the maximum is attributable to the K-absorption edges of tungsten (69.5 keV) and cadmium (26.7 keV), which lie within or immediately below this energy interval and locally enhance the photoelectric cross section. The retention of a high Z_eff at MeV energies makes A2 the only formulation of the series that offers useful attenuation for ^{137}Cs and ^{60}Co photons. For A3, Z_eff is almost independent of energy, varying by less than 0.5 % between 0.0595 and 1.332 MeV at 50 wt % (16.58 → 16.50); since copper and zinc have nearly identical atomic numbers and no absorption edge in the interval studied, the relative elemental contributions do not change with the interaction mechanism, and the composite behaves as a spectrally stable shield, although at a level below that of A2.

CONCLUSION

Three families of PMMA-based nanocomposites reinforced with $Zr(BH_4)_4$, $CdWO_4$ and Cu_3Zn_2 at 0, 5, 15, 25, 35 and 50 wt % were fabricated by cold pressing and characterized morphologically, chemically and with respect to their gamma-ray attenuation performance. The following conclusions are drawn. FE-SEM confirmed that all three fillers are dispersed in the matrix as nanometric particles, with mean sizes of 53–55 nm for $Zr(BH_4)_4$, 67–68 nm for $CdWO_4$ and 72–74 nm for Cu_3Zn_2, and without macroscopic voids or particle pull-out; the specimens therefore behave as effectively homogeneous media for the incident photons, which validates the mixture-rule treatment adopted in the calculations. FTIR spectroscopy showed that the characteristic PMMA bands (C=O at 1724–1725 cm^{-1}, C–O–C at 1147–1148 cm^{-1}, C–H and CH_3 modes) are retained unshifted, while the filler fingerprints (B–H at 2295 cm^{-1} and Zr–B at 1060 cm^{-1}; W–O–W at 878 cm^{-1}, W–O at 756 cm^{-1} and Cd–O at 622 cm^{-1}; Cu–O at 618 cm^{-1} and Zn–O at 522 cm^{-1}) appear without evidence of hydrolysis or matrix degradation. The stoichiometry assumed in the XCOM calculation is thus preserved in the real specimens, and the filler–matrix coupling is physical rather than covalent. The total linear attenuation coefficient increases with filler concentration and decreases with photon energy. The largest enhancement is obtained for the $CdWO_4$ system, whose μ at 0.0595 MeV grows from 0.2297 cm^{-1} for the unfilled matrix to 4.2092 cm^{-1} at 50 wt %, an increase by a factor of 18.3, and which remains the best attenuator up to 1.332 MeV. The effective atomic number follows the same ordering, reaching 33.62 for $CdWO_4$ at 0.093 MeV, 16.58 for Cu_3Zn_2 and 13.63 for $Zr(BH_4)_4$ at 50 wt %. The Cu_3Zn_2 composite exhibits a nearly energy-independent Z_eff (variation below 0.5 % between 0.0595 and 1.332 MeV), whereas Z_eff of the $Zr(BH_4)_4$ composite collapses to the value of the pure matrix above 0.3645 MeV. The $Zr(BH_4)_4$ system displays an anomalous, slight reduction of μ with increasing filler content above 0.3645 MeV, because the light boron and hydrogen atoms introduced with the borohydride lower the electron density of the composite in the energy region where Compton scattering, which depends linearly on Z, is the dominant interaction. This filler is therefore suitable for low-energy photon fields and for mixed neutron–gamma environments rather than for high-energy gamma shielding. Overall, the transition from photoelectric absorption at low energy to Compton scattering at intermediate energy accounts for all the observed trends, and the PMMA/$CdWO_4$ nanocomposite is identified as a lightweight, mouldable and non-toxic candidate for replacing lead-based shields in diagnostic radiology and low-energy gamma applications. Experimental transmission measurements with ^{241}Am, ^{137}Cs and ^{60}Co sources, together with mechanical and thermal testing of the optimum formulations, are recommended as the next stage of this work.

CONFLICT OF INTEREST

The authors declare that there is no conflict of interests regarding the publication of this manuscript.

REFERENCES

1. Pires LF, Medhat ME. Different methods of mass attenuation coefficient evaluation: Influences in the measurement of some soil physical properties. Applied Radiation and Isotopes. 2016;111:66-74.
2. Manohara SR, Hanagodimath SM, Thind KS, Gerward L. On the effective atomic number and electron density: A comprehensive set of formulas for all types of materials and energies above 1 keV. Nuclear Instruments and Methods in Physics Research Section B: Beam Interactions with Materials and Atoms. 2008;266(18):3906-3912.
3. Gowda S, Krishnaveni S, Yashoda T, Umesh TK, Gowda R. Photon mass attenuation coefficients, effective atomic

numbers and electron densities of some thermoluminescent dosimetric compounds. Pramana. 2004;63(3):529-541.
4. Oto B, Gür A. Determination of mass attenuation coefficients of concretes containing ulexite and ulexite concentrator waste. Ann Nucl Energy. 2013;59:72-74.
5. Biswas R, Sahadath H, Mollah AS, Huq MF. Calculation of gamma-ray attenuation parameters for locally developed shielding material: Polyboron. Journal of Radiation Research and Applied Sciences. 2016;9(1):26-34.
6. Gounhalli SG. Studies on Mass Attenuation Coefficient, Effective Atomic Numbers and Electron Densities of Some Narcotic Drugs in the Energy Range 1KeV -100GeV. IOSR Journal of Applied Physics. 2012;2(4):40-48.
7. Bullen DB. Radioactive Waste Management. J Environ Qual. 1991;20(1):316-316.
8. Norcia VD. Corporations and MoralityThomas Donaldson Englewood Cliffs, NJ: Prentice-Hall, 1982. Pp. ix, 214. $12.95, cloth; $8.95, paper - Business EthicsNorman Bowie Prentice-Hall Series in Occupational Ethics Englewood Cliffs, NJ: Prentice-Hall, 1982. Pp. xiii, 159. $7.95, paper. Dialogue. 1983;22(2):364-366.
9. Weinberg AW. Fundamental Aspects of Reactor Shielding . Herbert Goldstein. Addison-Wesley, Reading, Mass., 1959. xvi + 416 pp. $9.50. Science. 1959;130(3366):35-35.
10. Platzer N. Handbook of fillers for plastics, Harry S. Katz and John V. Milewski, Eds., Van Nostrand Reinhold, New York, 1987, 467 pp. Journal of Polymer Science: Polymer Letters Edition. 1988;26(6):274-274.
11. Srivatsan TS. A Review of: "Materials Processing and Texture, A. D. Rollett, (editor)". Mater Manuf Processes. 2009;24(10-11):1232-1233.
12. Mkhaiber A, Al-Bayati A, Fadhil I. Investigation Of Fast Neuron Attenuation Coefficients For Some Iraqi Building Materials. Malaysian Journal of Science. 2022;41(2):81-89.
13. Jackson DF, Hawkes DJ. X-ray attenuation coefficients of elements and mixtures. Phys Rep. 1981;70(3):169-233.
14. Chaiphaksa W, Limkitjaroenporn P, Kim HJ, Kaewkhao J. The mass attenuation coefficients, effective atomic numbers and effective electron densities for GAGG:Ce and CaMoO 4 scintillators. Prog Nuclear Energy. 2016;92:48-53.
15. Zenobio MAF, Zenobio EG, da Silva TA, Nogueira MdS. Effective atomic numbers (Zeff) of based calcium phosphate biomaterials: a comparative study. Applied Radiation and Isotopes. 2016;117:15-19.
16. Ali SM, Hassun HK, Salih AA, Athab RH, Al-Maiyaly BKH, Hussein BH. Study the properties of Cu2Se thin films for optoelectronic applications. Chalcogenide Letters. 2022;19(10):663-671.
17. Investigation Of $(Pb_2O_3)_x(SnO_2)_{1-x}$ Photon Shielding Capabilities For Medical Radiation Application. Journal of Radiation and Nuclear Applications. 2023;8(3):209-213.
18. Butkus M, Maciulyte-Sniukiene A, Matuzeviciute K, Davidaviciene V. Society's attitudes towards impact of immigration: case of EU countries. Marketing and Management of Innovations. 2018(1):338-352.
19. PERGAMON INTERNATIONAL LIBRARY of Science, Technology, Engineering and Social Studies. Computational Methods in Reactor Shielding: Elsevier; 1982. p. i. http://dx.doi.org/10.1016/b978-0-08-028685-3.50016-2
20. Crowley JM. Landscape Ecology, by R.T.T. Forman M. Godron. John Wiley and Sons, 605 Third Avenue, New York, NY 10158, USA: xix + 620 pp., figs and tables, 24 × 17 × 3.5 cm, hardbound, US $38.95, 1986. Environ Conserv. 1989;16(1):90-90.
21. Matthews FL. Stress Analysis of Fiber-Reinforced Composite Materials, M.W. Hyer, The McGraw Hill Companies, 1221 Avenue of the Americas, New York, NY 10020-1095, USA. 1997. 627pp. Illustrated. $90.75. The Aeronautical Journal. 1998;102(1014):220-220.
22. Flower HM. An Introduction to Composite Materials — Second edition D. Hull and T.W. Clyne Cambridge University Press, The Pitt Building, Trumpington Street, Cambridge CB2 IRP. 1996. 326pp. Illustrated. £19.95. The Aeronautical Journal. 1997;101(1005):228-228.
23. Gerward L, Guilbert N, Jensen KB, Levring H. WinXCom—a program for calculating X-ray attenuation coefficients. Radiat Phys Chem. 2004;71(3-4):653-654.